Pulse-Width Saturation and Kelly-Sideband Shift in a Graphene-Nanosheet Mode-Locked Fiber Laser with Weak Negative Dispersion

Chun-Yu Yang, Yung-Hsiang Lin, Yu-Chieh Chi, Chung-Lun Wu, Jui-Yung Lo, and Gong-Ru Lin*

Graduate Institute of Photonics and Optoelectronics, Department of Electrical Engineering, National Taiwan University, Number 1, Section 4, Roosevelt Road, Taipei 10617, Taiwan, Republic of China

(Received 8 December 2014; revised manuscript received 18 March 2015; published 24 April 2015)

The optimized soliton mode locking of the erbium-doped fiber laser (EDFL) and its pulse-shortening dynamic with the graphene nanosheet is demonstrated by precisely detuning the weakly negative group-delay dispersion (GDD) and maintaining strong self-phase-modulation (SPM), to obtain the shortest pulse width of 449 fs with a spectral linewidth of 6.02 nm. The pulse evolution with the mode-locking mechanism changing from the self-amplitude-modulation of the saturable absorber, to the soliton compression caused by the GDD and SPM is experimentally and numerically investigated in detail. Under high pumping powers, the enlarged up-chirp inside the EDFL cavity can induce a significant Kelly-sideband shift of up to 0.5 nm. The passively-mode-locked EDFL pulse width is controllable by detuning the GDD and SPM parameters, so that the pulse width can be compressed from 642 to 449 fs while reducing the negative GDD from -0.354 to -0.154 ps^2. The compression ratio can be also improved by strengthening the SPM at this stage.

DOI: 10.1103/PhysRevApplied.3.044016

I. INTRODUCTION

Passive mode locking of lasers via saturable absorbers (SAs) is a general mechanism to implement the ultrafast laser system. Recently, carbon-based materials have shown their great potential for being promising saturable absorbers for passively-mode-locked fiber lasers, such as single-walled carbon nanotubes (SWCNTs) [1–7], graphene [8–10], graphite [11,12], and charcoal nanoparticles [13]. At the initial stage, the SWCNT-incorporated saturable absorber has emerged with the advantages of an ultrafast relaxation time of <1 ps, a high optical damage threshold, a large optical nonlinearity, and polarization insensitivity [2–4]. However, the direct-band-gap SWCNT exhibits discrete working wavelengths corresponding to its diameter, which elucidates that the SWCNT does not always absorb light when the incoming optical wavelength is mismatched with any of the discrete band gaps. It causes linear loss only in the mismatched wavelength region. That is, the SWCNT with a unitary diameter hardly performs the property of broadband operation in passively-mode-locked fiber lasers, and the broadband absorption relies strictly on collecting the dispersed SWCNTs with different diameters in a single saturable absorber [4].

Since the investigation of mechanically exfoliated atomic-layer graphene by Novoselov *et al.* in 2004 [14], versatile synthesis methodologies for graphene saturable absorbers have also emerged [15–17]. The advantages of graphene, including broadband absorption, ultrafast relaxation, and low saturation intensity, make it a nice candidate of the low-threshold and wideband saturable absorber [15–17]. Hasan *et al.* demonstrated the first graphene mode-locked laser by synthesizing a polymer composite containing the exfoliated single- and few-layer graphene as the saturable absorber [18]. In addition, the atomic-layer graphene-based saturable absorber by using chemical vapor deposition (CVD) was further demonstrated by Bao *et al.* in 2009 [8]. The CVD-grown high-quality and large-area graphene can easily vary its layer number to provide an excellent saturable-absorption property for obtaining sub-ps pulse width from the passively-mode-locked erbium-doped fiber laser (EDFL) [19,20]. However, the CVD-grown graphene requires a rigorously controlled gaseous recipe, host matrix, and growth environment during synthesis. Various techniques are proposed for efficient synthesis of graphene materials, such as mechanical trituration [10,21], graphene-oxide reduction [22], and solution-based electrochemical exfoliation [23], etc. Among these demonstrations, the chemical solution process is considered to be the most economical way to quantitatively fabricate single- or few-layer nanoscale graphene materials in an aqueous environment, while maintaining the good quality for excellent passive mode locking.

According to the reports, the graphene saturable absorber possesses broadband absorption due to its zero-band-gap property, which has been experimentally characterized in passively-mode-locked or Q-switched lasers with wavelengths ranging from 800 to 3000 nm [24–29]. In passively-mode-locked EDFL, the graphene saturable absorber can

*Corresponding author.
grlin@ntu.edu.tw

also provide large wavelength tunability. Zhang *et al.* utilized graphene to adjust the wavelength from 1570 to 1600 nm for the dissipative soliton formed in an EDFL [30,31]. Sun *et al.* has demonstrated a tunable passively-mode-locked EDFL with a wavelength variable from 1525 to 1559 nm [32]. He *et al.* utilized a chirped-fiber Bragg grating to adjust the central wavelength of passively-mode-locked EDFL from 1539.4 to 1550 nm [33]. In addition, Huang *et al.* also demonstrated the generation of dissipative solitons in an all-normal-dispersion mode-locked Yb-doped fiber laser (YDFL), where the central wavelength can be shifted from 1051.8 to 1068.2 nm with a tuning range of 16.4 nm by changing the cavity birefringence [34].

Alternatively, the topological insulators (TIs), such as Bi_2Te_3 [35,36], Bi_2Se_3 [37], and MoS_2 [38], have also shown their potential to be broadband saturable absorbers due to their Dirac-like band structure. Several syntheses have been developed to fabricate these TI-based saturable absorbers, including CVD [39], mechanical cleavage [40], and the electrochemical solution process [41]. In particular, the electrochemical solution process can efficiently obtain the dispersed single- and few-layer TIs with nice quality. The broadband TI-based saturable absorbers can passively mode lock the lasers with a wavelength widely detuned from 800 to 1935 nm [42,43].

After mode locking, the soliton compression induced by the compensation between group delay dispersion (GDD) and self-phase-modulation (SPM) is commonly utilized for shortening the ultrafast laser pulse [44]. Popa *et al.* first introduced the soliton mode locking to generate the 174-fs short pulse by balancing the positive and negative cavity dispersion in the passively-mode-locked EDFL with the graphene saturable absorber [45]. By using soliton mode locking with the graphene-chitosan-solution-based saturable absorber, a 168-fs ultrafast passively-mode-locked EDFL can be obtained [46]. In addition, a soliton mode locking of EDFL with a pulse width of 455 fs can be also obtained by a nanoscale charcoal-powder-based saturable absorber [47]. Although soliton mode locking can further compress the laser pulse that originated from the self-amplitude-modulation (SAM) of a saturable absorber, the theoretical simulation as well as the parametric optimization have never been investigated in detail to achieve pulse compression in the carbon-material-based mode-locked EDFL systems previously.

In this work, the soliton mode locking of EDFL with a graphene-nanosheet saturable absorber obtained by precisely detuning the weakly negative GDD and maintaining the strong SPM is demonstrated. A convenient solution-based electrochemical exfoliation is utilized to effectively fabricate the graphene nanosheet. The soliton compression is experimentally optimized for obtaining the shortest EDFL pulse width, while the theoretical simulation is employed to elucidate the pulse-shaping mechanism.

II. EXPERIMENT

During electrochemical exfoliation, a highly oriented pyrolytic-graphite (HOPG) foil and a Pt wire are immersed in the electrolyte of a diluted sulfuric-acid solution to serve as the cathode and anode, respectively [12]. The graphene nanosheet can be exfoliated slowly and softly by applying the dc bias at a threshold voltage of +3 V. The average size of the graphene nanosheet is about 100 nm. However, the electrochemical exfoliation is inevitably accelerated by enlarging the bias up to +6 V. Under the stronger electrochemical exfoliation, the graphene nanosheets are rapidly torn from the HOPG foil, which massively produces large-size and multilayer graphene. In addition, several defects are concurrently induced outside the graphene nanosheets, such as bending, cracks, and vacancies [12]. Figure 1(a) provides a photograph of the electrochemical exfoliation process, and scanning-electron-microscopy (SEM) images of exfoliated graphene nanosheets with different sizes obtained at dc voltages of +3 and +6 V. In our previous work, we utilized atomic force microscopy (AFM) to directly measure the averaged layer number of graphene nanosheets fabricated by electrochemical exfoliation [48]. By applying the dc bias at a threshold voltage of +3 V to slowly exfoliate the graphene nanosheet, the average layer number of the graphene nanosheet ranges from 3 to 6. To accelerate the exfoliation of the graphene nanosheet by increasing the dc bias to +6 V, the average layer number of the graphene nanosheet enlarges to 22.

The Raman scattering spectra shown in Fig. 1(b) are used to examine the quality of the graphene nanosheets. For the graphene nanosheet with a lower layer number obtained at a dc voltage of +3 V, the *G*-mode Raman spectral peak at

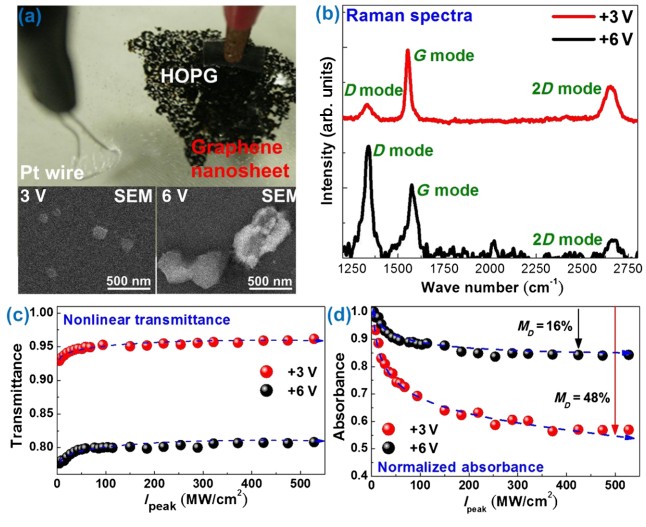

FIG. 1. (a) A photograph of the electrochemical exfoliation process and SEM images of graphene nanosheets obtained at dc voltages of +3 and +6 V. (b) The Raman scattering spectra. (c) Nonlinear transmittances. (d) Normalized absorbance of graphene nanosheets obtained at dc voltages of +3 and +6 V.

1552 cm^{-1} represents the vibration mode of the sp^2 carbon network, the D mode at 1330 cm^{-1} is caused by structural defects, and the $2D$ mode at 2650 cm^{-1} results from the overtone of the D mode [49,50]. Increasing the dc voltage to +6 V helps to obtain the multilayer graphene nanosheet with a larger size, in which the $2D$-mode-related Raman-scattering peak decreases its peak intensity and broadens its linewidth due to the increasing layer number. In contrast, the D-mode-related Raman scattering peak intensity is dramatically enlarged due to numerous structural defects generated on the surface of the graphene nanosheet.

Under the pumping of the pulsed laser with a pulse width of 700 fs at 1570 nm, the intensity-scan measurement is used to measure the nonlinear transmittances of the graphene nanosheet, as shown in Fig. 1(c). By increasing the illuminated intensity, the graphene nanosheet fabricated at an exfoliated bias of +3 V enlarges its transmittance T from 0.92 to 0.96 with a ΔT of 0.04, whereas the graphene nanosheet fabricated at an exfoliated bias of +6 V raises its transmittance from 0.77 to 0.8 with a ΔT of 0.03. A related equation $T = \exp[-\alpha_{\rm lin} - \alpha_{\rm non}/(1 + I_{\rm peak}/I_{\rm sat})]$ is employed to calculate the nonlinear transmittances, where $\alpha_{\rm lin}$, $\alpha_{\rm non}$, $I_{\rm peak}$, and $I_{\rm sat}$ denote the linear absorbance, nonlinear absorbance, input peak intensities, and saturation intensities of graphene nanosheets. A modulation coefficient γ representing the SAM effect is defined as $\alpha_{\rm non}/I_{\rm peak}$. The relative parameters for simulations are summarized in Fig. 2.

The parameters $\alpha_{\rm lin}$, $\alpha_{\rm non}$, and $I_{\rm sat}$ of graphene nanosheets obtained by 3 V (6 V) are 0.036 (0.21), 0.04 (0.044), and 66 (43), respectively. Both the graphene nanosheets exhibit similar $\alpha_{\rm non}$ and $I_{\rm sat}$; however, the $\alpha_{\rm lin}$ of a graphene nanosheet exfoliated at +3 V is much lower than that of a graphene nanosheet exfoliated at +6 V. Even though the graphene nanosheet exfoliated at +6 V reveals a lower nonsaturated transmittance (0.77) than that (0.92) of the graphene nanosheet exfoliated at +3 V, both the graphene nanosheets show a similar increment of their nonlinear transmittance. However, when transferring the nonlinear transmittance to the normalized absorbance as $\alpha_{\rm normalize} = [\alpha_{\rm lin} + \alpha_{\rm non}/(1 + I_{\rm peak}/I_{\rm sat})]_{\rm normalize} = [-\ln(T)]_{\rm normalize}$ and defining the modulation depth as $M_D = \gamma I_{\rm peak}/(\alpha_{\rm lin} + \alpha_{\rm non})$, by the decrement of normalized absorbance [8,51], the +3 and +6 V electrochemical exfoliation process causes the graphene nanosheets to demonstrate different saturable absorbances. As a result, the M_D contributed by the graphene nanosheet exfoliated at +3 V (48%) becomes higher than that of the graphene nanosheet exfoliated at +6 V (16%).

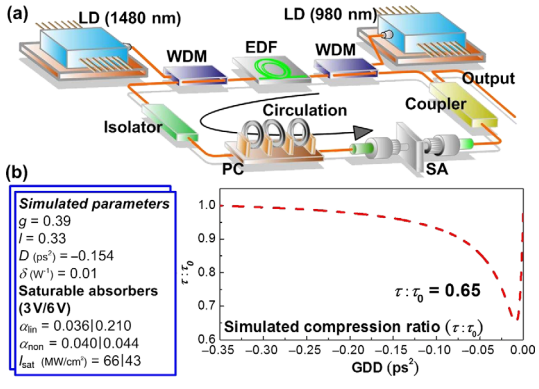

FIG. 2 (a) The configuration of the passively-mode-locked EDFL with a graphene nanosheet. (b) The simulated pulse width and compression ratio of the passively-mode-locked EDFL versus cavity GDD with the given parameters. (SA represents saturable absorber.)

III. SOLITON COMPRESSION

In principle, the obtained waveform from a passively-mode-locked EDFL cavity can be expressed by a sech function, derived from the master equation [52]. When considering the existences of GDD (D) and SPM (δ) inside the EDFL cavity to cause the phase shift of the field of the sech pulse envelope, the chirped sech function is modified as [53]

$$E(t) = A_0 \left[\mathrm{sech}\left(\frac{t}{\tau}\right)\right]^{(1+j\beta)} \exp(jw_0 t), \tag{1}$$

where β represents the chirp induced by the GDD and SPM effects, as given by

$$\beta = \frac{-3}{2}\left(\frac{\delta_n + D_n}{-1 + \delta_n D_n}\right) \pm \sqrt{\left[\frac{3}{2}\left(\frac{\delta_n + D_n}{-1 + \delta_n D_n}\right)\right]^2 + 2}, \tag{2}$$

where $\delta_n = \delta/\gamma$ denotes the normalized nonlinearity and $D_n = D/D_g$ (D_g, the gain and filter dispersion) denotes the normalized dispersion. With detuning the GDD and SPM inside the cavity, the pulse width τ_0 formed by the SAM of the saturable absorber will be modified to τ, as expressed by the following equation:

$$\tau = \frac{\tau_0}{2}(2 - \beta^2 - 3\beta D_n) = \tau_0\left[1 - \frac{\beta(\beta + 3D_n)}{2}\right]. \tag{3}$$

In the EDFL cavity with negative dispersion, except the chirp-free condition with $\beta = -3D_n$, the original pulse width τ_0 will be compressed with a factor of $[1 - \beta(\beta + 3D_n)/2]$ by incorporating the GDD and SPM. With a precise cavity design, including the sufficient pumping power and the appropriate fiber length, the strong nonlinear SPM effect by enlarging the intracavity pulse intensity can interact with the cavity dispersion to result in a significant soliton compression with an optimized ratio of 0.3.

As for an experimental demonstration, Fig. 2(a) illustrates the configuration of passively-mode-locked EDFL. The gain medium is a 2-m high-gain erbium-doped fiber

(EDF, nLIGHT Liekki Er80-8/125) with a corresponding dispersion coefficient $\beta_{2,\mathrm{EDF}}$ of -20 ps^2/km. The EDF is forward and backward pumped by a laser diode (LD) at 980 and 1480 nm, respectively, as delivered via two wavelength division multiplexing (WDM) couplers. When simultaneously increasing the pumping currents of two LDs up to 900 mA, the pumping powers of the 980- and 1480-nm LDs are enlarged to 290 and 200 mW, respectively. The direction of pulse circulation is determined by a nonpolarized optical isolator, and the cavity polarization is slightly detuned by a polarization controller (PC). A 1×2 optical coupler is utilized to provide a 95% feedback ratio and a 5% output ratio. The total length of the single-mode fiber (SMF) in the EDFL cavity is 5.7 m with the dispersion coefficient of $\beta_{2,\mathrm{SMF}} = -20$ ps^2/km; the EDF and SMF lead to the cavity GDD of -0.154 ps^2.

In order to construct a low-noise and high-gain L-band EDFA, the bidirectional pumping with the forward pumping of 980-nm LD and the backward pumping of 1480-nm LD is required. In comparison, the wavelength tuning range of a C-band EDFA is only 35 nm (from 1530 to 1565 nm), whereas the L-band EDFA easily covers the gain region from 1565 to 1625 nm. The forward pumping by 980-nm LD effectively suppresses the noise characteristics, while the better quantum conversion efficiency is provided by backward pumping with 1480-nm LD, as the pumping wavelength closer to the emission wavelength [54]. The small-signal gain g of the EDFL measured by an incident power of 0 dBm is about 3.9. The cavity loss l, excluding the saturable absorption of graphene nanosheets, is estimated to be 0.33. The SPM coefficient of $\delta = 0.01$ W^{-1} is calculated by $\delta = 2\pi n_2 L/\lambda_0 A_{\mathrm{eff}}$, where n_2 denotes the nonlinear refractive index, L the cavity length, λ_0 the EDFL wavelength, and A_{eff} the effective area. By substituting the cavity parameters and the nonlinear absorbance of graphene nanosheets into Eq. (3), the compression ratio $\tau : \tau_0$ can be obtained. That is, after initiating the EDFL pulse by the SAM, the peak intensity of the pulse is round-trip enlarged to induce the nonlinear SPM effect, such that the EDFL pulse will be shortened by a compression ratio of $\tau : \tau_0$. The corresponding parameters to simulate the variation of $\tau : \tau_0$ with different GDD are listed in Fig. 2(b). The value of $\tau : \tau_0$ is slightly decreased with increasing GDD from -0.35 to -0.01 ps^2, and the pulse is significantly compressed with a $\tau : \tau_0$ minimum of 0.65 by designing the EDFL cavity at a weakly negative GDD of -0.01 ps^2.

IV. PULSE-WIDTH SATURATION AND KELLY-SIDEBAND SHIFT

To identify the dominated mode-locking mechanism, the evolutions on autocorrelation trace and optical spectrum with increasing pumping powers are demonstrated in Fig. 3. By simultaneously increasing the pumping currents of two LDs from 100 to 900 mA, the pumping powers of the 980- and 1480-nm LDs are enlarged from 30 to 290 mW, and from 0.1 to 200 mW, respectively. When providing the maximum pumping powers to the EDFL cavity, both the graphene-nanosheet samples obtained by +3 and +6 V can stably initiate the passive mode locking in the EDFL. However, the graphene-nanosheet samples obtained at a lower voltage present a shorter pulse and broader spectrum, accompanied by a stronger Kelly-sideband intensity. The enhanced Kelly sideband is treated as distinct evidence for the stronger pulse-shortening force with a higher nonlinear saturable absorbance as well as a larger modulation depth induced by the graphene nanosheet with a few layers.

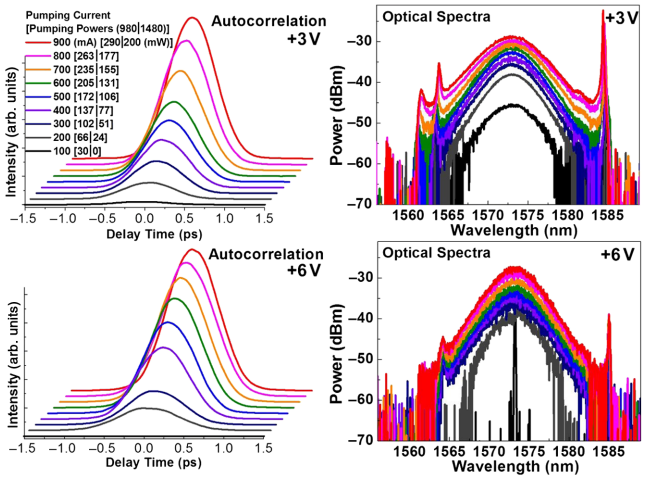

FIG. 3. The autocorrelation traces and optical spectra of the passively-mode-locked EDFLs at different pumping powers with graphene nanosheets obtained by using the dc voltages of +3 and +6 V.

As evidence, Fig. 4 depicts the varied pulse width and spectral linewidth of the passively-mode-locked EDFLs with increasing pumping powers. For the EDFL passively mode locked by graphene nanosheets with fewer layers, the shorter pulse width is obtained and can be narrowed from 494 to 449 fs, accompanied by a broadening spectral linewidth from 5.23 to 6.02 nm by increasing the pumping

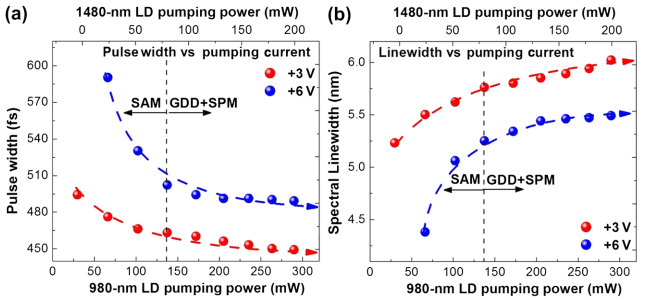

FIG. 4. (a) The variations of pulse width and (b) spectral linewidth of the passively-mode-locked EDFLs at different pumping powers with the graphene nanosheets obtained by using the dc voltages of +3 and +6 V.

currents of two LDs from 100 to 900 mA [Fig. 4(a)]. In contrast, the EDFL passively mode locked by graphene nanosheets with more layers can only shorten its pulse width from 589 to 489 fs and broaden its linewidth from 4.38 to 5.49 nm [Fig. 4(b)]. The observed time-bandwidth products of all of the EDFLs are around 0.32, and the mode locking seems to reveal a weaker dependence with the layer number of the graphene samples at larger pumping conditions. According to Fig. 4, the passively-mode-locked EDFLs with different graphene-nanosheet-based saturable absorbers dramatically shorten their pulse width with increasing the pumping currents of two LDs from 100 to 400 mA. In the SAM region, the passively-mode-locked EDFL pulse width is inversely related to the intracavity pulse intensity [40,48]. That is, the enlarged pulse intensity is a dominant factor on the decreasing trends of pulse-width shortening.

In contrast, both the decreasing trends of EDFL pulse width in both cases become slower by increasing the pumping currents from 400 to 600 mA, where the passively-mode-locked EDFL with few-layer and multilayer graphene nanosheets maintain the pulse width of 456 and 491 fs, respectively. When exceeding the pumping currents to 400 mA (980-nm LD of 137 mW; 1480-nm LD of 77 mW) or larger, the refractive index of SMF and EDF are increased due to their positive nonlinear refractive index under the operation of high pulse intensity. In our case, the average output power of the passively-mode-locked EDFL with a few-layer graphene nanosheet is about 3.5 mW, so that the corresponding intracavitiy peak intensity is 6.9 GW/cm^2. The increased nonlinear refractive index of $\Delta n = n_2 I_{\text{peak}}$ can be calculated as 4×10^{-6} ($n_2 = n_{2,\text{SMF}} + n_{2,\text{EDF}} = 5.9 \times 10^{-16}$ cm^2/W, where $n_{2,\text{SMF}} = 2.9 \times 10^{-16}$ cm^2/W, and $n_{2,\text{EDF}} = 3 \times 10^{-16}$ cm^2/W) [55,56]. The increased nonlinear refractive index results in an intensity-dependent phase shift to induce the frequency chirp. The positive chirp (up-chirp) caused by the SPM will enlarge its magnitude with the 7.7-m fiber to induce the SPM coefficient δ of 0.01 W^{-1}. However, the frequency chirp caused by the GDD is negative (down-chirp), which effectively compensates the opposite chirp from the SPM to form a chirp-suppressed pulse in the EDFL cavity [57]. These pulse evolutions confirm the possibility that the pulse-shortening mechanism effectively changes from the SAM of the saturable absorber to the soliton compression induced by GDD and SPM at large intercavity pulse intensity.

Note that the compensation between chirp and dispersion of a pulse could also affect the feature of the Kelly sideband. In the experiment, the peak wavelength of first-order Kelly-sideband signals tends to move closer toward the mode-locking spectrum at higher pumping powers. Theoretically, the shift of the peak-frequency spacing of the Nth-ordered Kelly sideband $\Delta v_{\text{Kelly},N}$ is a function of both GDD and pulse-width variations, as described by [58,59]

$$\Delta v_{\text{Kelly},N} \approx \frac{\ln(1+\sqrt{2})}{\pi} \sqrt{\frac{4N}{|\beta_{2,\text{eff}}|L} - \frac{1}{\tau_s^2}}, \tag{4}$$

where $\beta_{2,\text{eff}}$ and L are the effective dispersion coefficient and cavity length. Because of the concurrent existence of the SPM and pulse compression effects, the shift of the Kelly-sideband frequency is given as

$$\begin{aligned}\delta\Delta v_{\text{Kelly},N} &= \frac{\Delta v_{\text{Kelly},N}}{2}\left(\frac{4N}{|\beta_{2,\text{eff}}|L} - \frac{1}{\tau_s^2}\right)^{-1}\left(\frac{1}{\tau_s^3}\delta\tau_s - \frac{4NL}{(|\beta_{2,\text{eff}}|L)^2}\delta|\beta_{2,\text{eff}}|\right) \\ &= -\frac{\Delta v_{\text{Kelly},N}}{2}\left(\frac{4N}{|\beta_{2,\text{eff}}|L} - \frac{1}{\tau_s^2}\right)^{-1}\left(\frac{1}{\tau_s^2}\frac{\delta\tau_s}{\tau_s} - \frac{4N}{(|\beta_{2,\text{eff}}|L)}\frac{\delta|\beta_{2,\text{eff}}|}{|\beta_{2,\text{eff}}|}\right).\end{aligned} \tag{5}$$

In Eq. (5), the frequency shift of the Kelly sideband is dominated by the soliton pulse width and the effective GDD, which are affected by the compensation between chirp and dispersion of the circulated pulse. The maximal blueshift of the Kelly sideband at the long-wavelength side can be up to 0.5 nm (see Fig. 5), indicating that a significant prechirping has been added to the circulated pulse with enlarging the pumping power as well as pulse intensity.

The generation of the Kelly sideband is induced by the constructive interference of the soliton pulse and dispersive waves [51,58,59]. Both the graphene saturable absorber and the conventional nonlinear-polarization-rotation (NPR) technique can generate soliton mode locking with Kelly

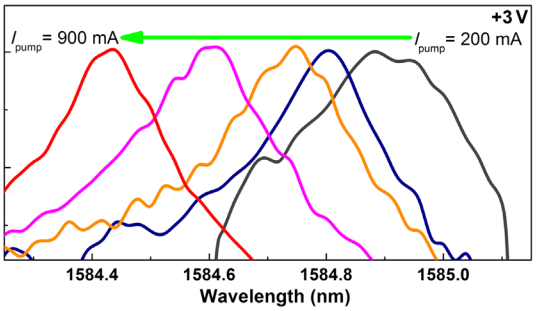

FIG. 5. The shift of the Kelly-sideband peak in the pulse spectrum of the passively-mode-locked EDFL with a graphene nanosheet obtained by +3 V under different pumping power.

sidebands. In principle, the Kelly sidebands can be effectively suppressed in a purely NPR-mode-locked EDFL system [60], whereas it always exists in the soliton spectrum of purely saturable-absorber mode-locked EDFL. To characterize if the graphene saturable absorber itself contributes the shifting or location of the Kelly sidebands, the passive mode-locking spectra of the same EDFL system without (by weak NPR effect) and with (by saturable-absorption effect) intracavity graphene nanosheets are measured, as shown in Fig. 6. Without a graphene saturable absorber, the soliton with a pulse width of $\tau_{s,\mathrm{NPR}} = 460$ fs shows a Kelly-sideband spectrum with a frequency spacing of $\Delta\upsilon_{\mathrm{NPR}} = 1.47$ THz. With the graphene saturable absorber, the soliton with a pulse width of $\tau_{s,\mathrm{graphene}} = 449$ fs shows a Kelly-sideband spectrum with a frequency spacing of $\Delta\upsilon_{\mathrm{graphene}} = 1.4$ THz. For the NPR-based passively-mode-locked EDFL system, the calculated effective GDD ($|\beta_{2,\mathrm{eff}}|L$) from Eq. (4) is about -0.124 ps^2 (where $\Delta\upsilon_{\mathrm{NPR}} = 1.47$ THz, $\tau_{s,\mathrm{NPR}} = 460$ fs). After adding the graphene nanosheet into the EDFL cavity, the calculated effective GDD is changed to -0.134 ps^2 (where $\Delta\upsilon_{\mathrm{graphene}} = 1.4$ THz, $\tau_{s,\mathrm{graphene}} = 449$ fs). Since two SMF patch cords with a total length of 50 cm are used to sandwich the graphene, an additional GDD of -0.01 ps^2 ($\beta_{2,\mathrm{eff}}L = 50$ cm $\times -20$ ps^2/km) has to be added into the effective GDD. That is, the increment on the effective GDD of the graphene-nanosheet mode-locked EDFL system is mainly attributed to the SMF patch cord but not to the graphene. Although graphene possesses a significant Kerr nonlinearity of $n_2 \sim 10^{-7}$ cm^2/W, it is 9 orders of magnitude larger than SMF and EDF [61]. However, the thickness of single-layer graphene L_g is only ~0.34 nm. When taking the thickness of graphene into account, the SPM coefficient of graphene with thickness L_g is $\delta_{\mathrm{graphene}} = 2 \times 10^{-4}$ W^{-1}, which is 2 orders of magnitude smaller than that contributed by intracavity fibers ($\delta_{\mathrm{SMF+EDF}} = 1 \times 10^{-2}$ W^{-1}).

Consequently, the pulse-width narrowing effect shows a limitation with enlarging the pumping currents from 600 to 900 mA, indicating that the soliton shaping no longer becomes sensitive to the further increase on pumping power. Because the enhancement of soliton peak intensity is limited by the soliton-area theorem derived from a NPR mode-locked fiber laser system with an empirical equation of $A_0\tau = (2|D|/\delta)^{1/2}$, the interaction of GDD (D) and SPM (δ) maintains the product of peak amplitude A_0 and pulse width τ as a constant [59]. When the pumping power is enhanced to increase the soliton peak intensity, the peak intensity of the pulse will be eventually saturated to split the single-soliton pulse into multiple pulses [56,62]. Therefore, the SPM effect will not become stronger under the operation of high pumping powers to influence the soliton pulse shape and intensity.

On the other hand, when considering the GDD and SPM as the main factors for shaping the soliton pulse under high pumping powers, the pulse width τ of the passively-mode-locked EDFL should be controllable with detuning the cavity parameters of D and δ. Inserting an additional SMF into the cavity is a convenient method to directly detune the cavity parameters including D and δ. Figure 7(a) demonstrates the pulse-width variation of the passively-mode-locked EDFL with a few-layer graphene nanosheet by changing the SMF length. By fixing the EDF length of 2 m and reducing the SMF length from 15.7 to 5.7 m, the negative GDD increases from -0.354 to -0.154 ps^2 to shorten the EDFL pulse width from 642 to 449 fs. The experimental results are well correlated with the theoretical results. Furthermore, the pulse-width compression ratio under the soliton shaping procedure is only a function of D

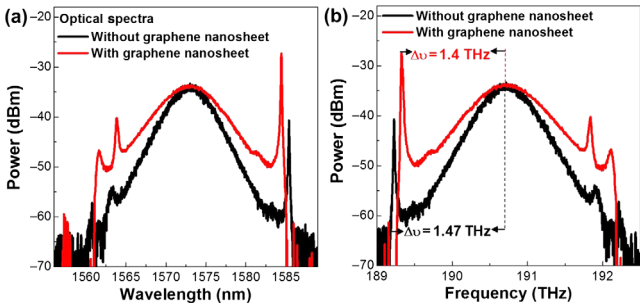

FIG. 6 (a) The optical spectra of the passively-mode-locked EDFLs with and without the graphene nanosheet in the wavelength domain. (b) The optical spectra of the passively-mode-locked EDFLs with and without the graphene nanosheet in the frequency domain.

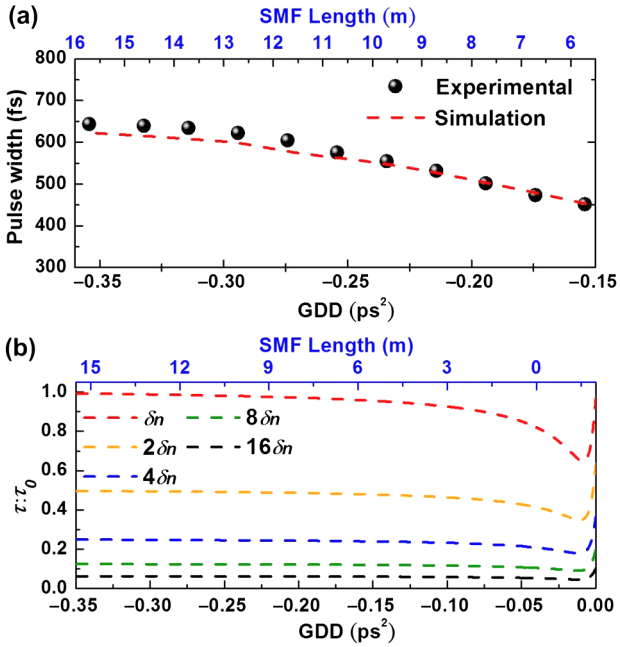

FIG. 7. (a) The experimental and simulated pulse-width variation versus different GDD by changing the SMF length. (b) The simulated compression ratio $\tau:\tau_0$ versus different GDD under the altering δ_n coefficients.

and δ but not directly affected by the pulse intensity. Figure 7(b) shows the improved compression ratio with enlarging the normalized nonlinearity δ_n. The optimized compression ratio can be lowered down to 0.35 by doubling the δ_n. In principle, the compression ratio is further strengthened to 0.045 by enhancing the δ_n to 16 times, which strictly depends on realistically enhancing the circulated pulse intensity with enlarging pumping power. The decreasing trend of the compression ratio slows down with the increasing δ_n. The optimized compression ratios with different δ_n occur at $D = -0.01$ ps^2.

V. CONCLUSION

In conclusion, the pulse-shortening dynamics of an EDFL soliton system mode locked with the graphene-nanosheet saturable absorber are experimentally and numerically analyzed in this work. The EDFL pulse is initiated with the electrochemically exfoliated graphene-nanosheet samples obtained by a convenient solution process, which can be further compressed by precisely detuning the weakly negative GDD and maintaining the strong SPM. The enhanced SPM effect increases the nonlinear refractive index of intracavity fiber to result in the intensity-dependent phase shift as well as the frequency up-chirp, whereas the negative GDD effectively compensates the opposite chirp to form a chirp-suppressed pulse. In particular, the enlarged up-chirp further induces a significant Kelly-sideband shift of up to 0.5 nm when operating the EDFL at high pumping powers. The passively-mode-locked EDFL with a few-layer graphene nanosheet can shorten the pulse width to 449 fs with a corresponding linewidth of 6.02 nm. The SAM mechanism dramatically shortens the passively-mode-locked EDFL pulse width with increasing the LD pumping current to 400 mA, whereas the SPM takes over the pulse-shortening procedure to the soliton regime by further increasing the LD current. Under high pumping powers, the EDFL pulse width is controllable with detuning the cavity parameters of D and δ. By reducing the SMF length from 15.7 to 5.7 m, the negative GDD decreases from -0.354 to -0.154 ps^2 so as to further compress the EDFL pulse width from 642 to 449 fs. The compression ratio can be improved by strengthening the SPM at this stage; however, a unique phenomenon occurs to cease the pulse-width compression at LD pumping current beyond 600 mA. The SPM effect no longer affects the soliton pulse shape and intensity at high pumping powers, because the enhancement of soliton peak intensity is limited as predicted by the soliton-area theorem. The optimized compression ratios with different δ_n occur at $D = -0.01$ ps^2.

ACKNOWLEDGMENTS

This work was supported by the Ministry of Science and Technology, Taiwan, Republic of China, and the Excellent Research Projects of National Taiwan University, Taiwan, under Grants No. NSC 100-2221-E-002-156-MY3, No. NSC 101-2221-E-002-071-MY3, No. MOST 103-2221-E002-042-MY3, and No. NTU104R89083.

[1] S. Y. Set, H. Yaguchi, Y. Tanaka, and M. Jablonski, Ultrafast fiber pulsed lasers incorporating carbon nanotubes, IEEE J. Sel. Top. Quantum Electron. **10**, 137 (2004).
[2] S. Y. Set, H. Yaguchi, Y. Tanaka, and M. Jablonski, Laser mode locking using a saturable absorber incorporating carbon nanotubes, J. Lightwave Technol. **22**, 51 (2004).
[3] S. Yamashita, Y. Inoue, S. Maruyama, Y. Murakami, H. Yaguchi, M. Jablonski, and S. Y. Set, Saturable absorbers incorporating carbon nanotubes directly synthesized onto substrates and fibers and their application to mode-locked fiber lasers, Opt. Lett. **29**, 1581 (2004).
[4] F. Wang, A. G. Rozhin, V. Scardaci, Z. Sun, F. Hennrich, I. H. White, W. I. Milne, and A. C. Ferrari, Wideband-tunable, nanotube mode-locked, fibre laser, Nat. Nanotechnol. **3**, 738 (2008).
[5] T. Hasan, Z. Sun, F. Wang, F. Bonaccorso, P. H. Tan, A. G. Rozhin, and A. C. Ferrari, Nanotube-polymer composites for ultrafast photonics, Adv. Mater. **21**, 3874 (2009).
[6] K.-N. Cheng, Y.-H. Lin, S. Yamashita, and G.-R. Lin, Harmonic order dependent pulsewidth shortening of a passively mode-locked fiber laser with carbon nanotube saturable absorber, IEEE Photonics J. **4**, 1542 (2012).
[7] K.-N. Cheng, Y. H. Lin, and G.-R. Lin, Single- and double-walled carbon nanotube based saturable absorbers for passive mode-locking of an erbium-doped fiber laser, Laser Phys. **23**, 045105 (2013).
[8] Q. Bao, H. Zhang, Z. Ni, Y. Yan, Z. X. Shen, K. P. Loh, and D. Y. Tang, Atomic-layer graphene as a saturable absorber for ultrafast pulsed lasers, Adv. Funct. Mater. **19**, 3077 (2009).
[9] Z. Sun, T. Hasan, F. Torrisi, D. Popa, G. Privitera, F. Wang, F. Bonaccorso, D. M. Basko, and A. C. Ferrari, Graphene mode-locked ultrafast laser, ACS Nano **4**, 803 (2010).
[10] A. Martinez, K. Fuse, and S. Yamashita, Mechanical exfoliation of graphene for the passive mode-locking of fiber lasers, Appl. Phys. Lett. **99**, 121107 (2011).
[11] Y. H. Lin and G.-R. Lin, Free-standing nano-scale graphite saturable absorber for passively mode-locked erbium doped fiber ring laser, Laser Phys. Lett. **9**, 398 (2012).
[12] Y. H. Lin, C.-Y. Yang, J. H. Liou, C. P. Yu, and G.-R. Lin, Using graphene nano-particle embedded in photonic crystal fiber for evanescent wave mode-locking of fiber laser, Opt. Express **21**, 16763 (2013).
[13] Y. H. Lin, Y. C. Chi, and G.-R. Lin, Nanoscale charcoal powder induced saturable absorption and mode-locking of a low-gain erbium-doped fiber-ring laser, Laser Phys. Lett. **10**, 055105 (2013).
[14] K. S. Novoselov, A. K. Geim, S. V. Morozov, D. Jiang, Y. Zhang, S. V. Dubonos, I. V. Grigorieva, and A. A. Firsov, Electric field effect in atomically thin carbon films, Science **306**, 666 (2004).

[15] F. Bonaccorso, Z. Sun, T. Hasan, and A. C. Ferrari, Graphene photonics and optoelectronics, Nat. Photonics **4**, 611 (2010).

[16] Z. Sun, T. Hasan, and A. C. Ferrari, Ultrafast lasers mode-locked by nanotubes and graphene, Physica (Amsterdam) **44E**, 1082 (2012).

[17] A. Martinez and Z. Sun, Nanotube and graphene saturable absorbers for fibre laser, Nat. Photonics **7**, 842 (2013).

[18] T. Hasan, Z. Sun, F. Wang, F. Bonaccorso, P. H. Tan, A. G. Rozhin, and A. C. Ferrari, Nanotube-polymer composites for ultrafast photonics, Adv. Mater. **21**, 3874 (2009).

[19] P. L. Huang, S.-C. Lin, C.-Y. Yeh, H.-H. Kuo, S.-H. Huang, G.-R. Lin, L.-J. Li, C.-Y. Su, and W.-H. Cheng, Stable mode-locked fiber laser based on CVD fabricated graphene saturable absorber, Opt. Express **20**, 2460 (2012).

[20] G. Sobon, J. Sotor, I. Pasternak, A. Krajewska, W. Strupinski, and K. M. Abramski, Thulium-doped all-fiber laser mode-locked by CVD-graphene/PMMA saturable absorber, Opt. Express **21**, 12797 (2013).

[21] G.-R. Lin and Y.-C. Lin, Directly exfoliated and imprinted graphite nano-particle saturable absorber for passive mode-locking erbium-doped fiber laser, Laser Phys. Lett. **8**, 880 (2011).

[22] G. Sobon, J. Sotor, J. Jagiello, R. Kozinski, M. Zdrojek, M. Holdynski, P. Paletko, J. Boguslawski, L. Lipinska, and K. M. Abramski, Graphene oxide vs. reduced graphene oxide as saturable absorbers for Er-doped passively mode-locked fiber laser, Opt. Express **20**, 19463 (2012).

[23] F. Bonaccorso and Z. Sun, Solution processing of graphene, topological insulators and other 2d crystals for ultrafast photonics, Opt. Mater. Express **4**, 63 (2014).

[24] I. H. Baek, H. W. Lee, S. Bae, B. H. Hong, Y. H. Ahn, D. I. Yeom, and F. Rotermund, Efficient mode-locking of sub-70-fs Ti:sapphire laser by graphene saturable absorber, Appl. Phys. Express **5**, 032701 (2012).

[25] X. H. Li, Y. G. Wang, Y. S. Wang, Y. Z. Zhang, K. Wu, P. P. Shum, X. Yu, Y. Zhang, and Q. J. Wang, All-normal-dispersion passively mode-locked Yb-doped fiber ring laser based on a graphene oxide saturable absorber, Laser Phys. Lett. **10**, 075108 (2013).

[26] Y. H. Lin, C. Y. Yang, S. F. Lin, and G-R. Lin, Triturating versatile carbon materials as saturable absorptive nano powders for ultrafast pulsating of erbium-doped fiber lasers, Opt. Mater. Express **5**, 236 (2015).

[27] A. A. Lagatsky, Z. Sun, T. S. Kulmala, R. S. Sundaram, S. Milana, F. Torrisi, O. L. Antipov, Y. Lee, J. H. Ahn, C. T. A. Brown, W. Sibbett, and A. C. Ferrari, 2 μm solid-state laser mode-locked by single-layer graphene, Appl. Phys. Lett. **102**, 013113 (2013).

[28] N. Tolstik, E. Sorokin, and I. T. Sorokina, Graphene mode-locked Cr:ZnS laser with 41 fs pulse duration, Opt. Express **22**, 5564 (2014).

[29] G. Zhu, X. Zhu, K. Balakrishnan, R. A. Norwood, and N. Peyghambarian, Fe^{2+}:ZnSe and graphene Q-switched singly Ho^{3+}-doped ZBLAN fiber lasers at 3 μm, Opt. Mater. Express **3**, 1365 (2013).

[30] H. Zhang, D. Y. Tang, L. M. Zhao, Q. Bao, K. P. Loh, B. Lin, and S. C. Tjin, Compact graphene mode-locked wavelength-tunable erbium-doped fiber lasers: From all anomalous dispersion to all normal dispersion, Laser Phys. Lett. **7**, 591 (2010).

[31] H. Zhang, D. Y. Tang, R. J. Knize, L. Zhao, Q. Bao, and K. P. Loh, Graphene mode locked, wavelength-tunable, dissipative soliton fiber laser, Appl. Phys. Lett. **96**, 111112 (2010).

[32] Z. Sun, D. Popa, T. Hasan, F. Torrisi, F. Wang, E. J. R. Kelleher, J. C. Travers, V. Nicolosi, and A. C. Ferrari, A stable, wideband tunable, near transform-limited, graphene mode-locked, ultrafast laser, Nano Res. **3**, 653 (2010).

[33] X. He, Z. Liu, and D. N. Wang, Wavelength-tunable, passively mode-locked fiber laser based on graphene and chirped fiber Bragg grating, Opt. Lett. **37**, 2394 (2012).

[34] S. Huang, Y. Wang, P. Yan, J. Zhao, H. Li, and R. Lin, Tunable and switchable multi-wavelength dissipative soliton generation in a graphene oxide mode-locked Yb-doped fiber laser, Opt. Express **22**, 11417 (2014).

[35] C. Zhao, H. Zhang, X. Qi, Y. Chen, Z. Wang, S. Wen, and D. Y. Tang, Ultra-short pulse generation by a topological insulator based saturable absorber, Appl. Phys. Lett. **101**, 211106 (2012).

[36] Y. H. Lin, C. Y. Yang, S. F. Lin, W. H. Tseng, Q. Bao, C. I. Wu, and G.-R. Lin, Soliton compression of the erbium-doped fiber laser weakly started mode-locking by nanoscale p-type Bi_2Te_3 topological insulator particles, Laser Phys. Lett. **11**, 055107 (2014).

[37] C. Zhao, Y. Zou, Y. Chen, Z. Wang, S. Lu, H. Zhang, S. Wen, and D. Y. Tang, Wavelength-tunable picosecond soliton fiber laser with topological insulator: Bi_2Se_3 as a mode locker, Opt. Express **20**, 27888 (2012).

[38] H. Zhang, S. B. Lu, J. Zheng, J. Du, S. C. Wen, D. Y. Tang, and K. P. Loh, Molybdenum disulfide (MoS_2) as a broadband saturable absorber for ultra-fast photonics, Opt. Express **22**, 7249 (2014).

[39] Y.-H. Lee, X.-Q. Zhang, W. Zhang, M.-T. Chang, C.-T. Lin, K.-D. Chang, Y.-C. Yu, J. T.-W. Wang, C.-S. Chang, L.-J. Li, and T.-W. Lin, Synthesis of large-area MoS_2 atomic layers with chemical vapor deposition, Adv. Mater. **24**, 2320 (2012).

[40] K. F. Mak, C. Lee, J. Hone, J. Shan, and T. F. Heinz, Atomically Thin MoS_2: A New Direct-Gap Semiconductor, Phys. Rev. Lett. **105**, 136805 (2010).

[41] R. J. Smith, P. J. King, M. Lotya, C. Wirtz, U. Khan, S. De, A. O'Neill, G. S. Duesberg, J. C. Grunlan, G. Moriarty, J. Chen, J. Wang, A. I. Minett, V. Nicolosi, and J. N. Coleman, Large-scale exfoliation of inorganic layered compounds in aqueous surfactant solutions, Adv. Mater. **23**, 3944 (2011).

[42] S. Chen, C. Zhao, Y. Li, H. Huang, S. Lu, H. Zhang, and S. Wen, Broadband optical and microwave nonlinear response in topological insulator, Opt. Mater. Express **4**, 587 (2014).

[43] M. Jung, J. Lee, J. Koo, J. Park, Y. W. Song, K. Lee, S. Lee, and J. H. Lee, A femtosecond pulse fiber laser at 1935 nm using a bulk-structured Bi_2Te_3 topological insulator, Opt. Express **22**, 7865 (2014).

[44] F. X. Kartner, I. D. Jung, and U. Keller, Soliton mode-locking with saturable absorbers, IEEE J. Sel. Top. Quantum Electron. **2**, 540 (1996).

[45] D. Popa, Z. Sun, F. Torrisi, T. Hasan, F. Wang, and A. C. Ferrari, Sub 200 fs pulse generation from a graphene mode-locked fiber laser, Appl. Phys. Lett. **97**, 203106 (2010).

[46] J. Tarka, G. Sobon, J. Boguslawski, J. Sotor, J. Jagiello, M. Aksienionek, L. Lipinska, M. Zdrojek, J. Judek, and K. M. Abramski, 168 fs pulse generation from graphene-chitosan mode-locked fiber laser, Opt. Mater. Express **4**, 1981 (2014).

[47] Y. H. Lin, J. Y. Lo, W. H. Tseng, C.-I. Wu, and G.-R. Lin, Self-amplitude and self-phase modulation of the charcoal mode-locked erbium-doped fiber lasers, Opt. Express **21**, 25184 (2013).

[48] C. Y. Yang, C.-L. Wu, Y. H. Lin, L. H. Tsai, Y.-C. Chi, J. H. Chang, C.-I. Wu, H.-K. Tsai, D. P. Tsai, and G.-R. Lin, Fabricating graphite nano-sheet powder by slow electrochemical exfoliation of large-scale graphite foil as a mode-locker for fiber lasers, Opt. Mater. Express **3**, 1893 (2013).

[49] L. M. Malard, M. A. Pimenta, G. Dresselhaus, and M. S. Dresselhaus, Raman spectroscopy in graphene, Phys. Rep. **473**, 51 (2009).

[50] A. C. Ferrari, J. C. Meyer, V. Scardaci, C. Casiraghi, M. Lazzeri, F. Mauri, S. Piscanec, D. Jiang, K. S. Novoselov, S. Roth, and A. K. Geim, Raman Spectrum of Graphene and Graphene Layers, Phys. Rev. Lett. **97**, 187401 (2006).

[51] Y. H. Lin and G.-R. Lin, Kelly sideband variation and self four-wave-mixing in femtosecond fiber soliton laser mode-locked by multiple exfoliated graphite nano-particles, Laser Phys. Lett. **10**, 045109 (2013).

[52] H. A. Haus, Mode-locking of lasers, IEEE J. Sel. Top. Quantum Electron. **6**, 1173 (2000).

[53] F. X. Kaertner, "Mode-locked laser theory," 2006.

[54] H. Ono, M. Yamada, T. Kanamori, S. Sudo, and Y. Ohishi, 1.58-μm band gain-flattened erbium-doped fiber amplifiers for WDM transmission systems, J. Lightwave Technol. **17**, 490 (1999).

[55] T. Kato, Y. Suetsugu, M. Takagi, E. Sasaoka, and M. Nishimura, Measurement of the nonlinear refractive index in optical fiber by the cross-phase-modulation method with depolarized pump light, Opt. Lett. **20**, 988 (1995).

[56] T. Hieta and E. Ikonen, Measurement of Er-doped fiber nonlinearity using continuous-wave self-phase modulation method, J. Lightwave Technol. **27**, 2977 (2009).

[57] G. P. Agrawal, *Nonlinear Fiber Optics* (Academic Press, San Diego, CA, 2001).

[58] S. M. J. Kelly, Characteristic sideband instability of periodically amplified average soliton, Electron. Lett. **28**, 806 (1992).

[59] L. E. Nelson, D. J. Jones, K. Tamura, H. A. Haus, and E. P. Ippen, Ultrashort-pulse fiber ring lasers, Appl. Phys. B **65**, 277 (1997).

[60] Z. C. Luo, A. P. Luo, W. C. Xu, C. X. Song, Y. X. Gao, and W. C. Chen, Sideband controllable soliton all-fiber ring laser passively mode-locked by nonlinear polarization rotation, Laser Phys. Lett. **6**, 582 (2009).

[61] H. Zhang, S. Virally, Q. Bao, L. K. Ping, S. Massar, N. Godbout, and P. Kockaert, *Z*-scan measurement of the nonlinear refractive index of graphene, Opt. Lett. **37**, 1856 (2012).

[62] Y. Chen, M. Wu, P. Tang, S. Chen, J. Du, G. Jiang, Y. Li, C. Zhao, H. Zhang, and S. Wen, The formation of various multi-soliton patterns and noise-like pulse in a fiber laser passively mode-locked by a topological insulator based saturable absorber, Laser Phys. Lett. **11**, 055101 (2014).